Laser and Particle Beams (2012), *30*, 57–63.

doi:10.1017/S0263034611000681

Nano-structuring of solid surface by extreme ultraviolet Ar^{8+} laser

K. KOLACEK,[1] J. STRAUS,[1] J. SCHMIDT,[1] O. FROLOV,[1] V. PRUKNER,[1] A. SHUKUROV,[2] V. HOLY,[2] J. SOBOTA,[3] AND T. FORT[3]

[1]Institute of Plasma Physics, Academy of Sciences of the Czech Republic, Prague, Czech Republic
[2]Faculty of Mathematics and Physics, Charles University in Prague, Czech Republic
[3]Institute of Scientific Instruments, Academy of Sciences of the Czech Republic, Brno, Czech Republic

(RECEIVED 2 June 2011; ACCEPTED 26 October 2011)

Abstract

This work demonstrates the patterning of polymethylmethacrylate (PMMA) by ablation with Ar^{8+} ion laser ($\lambda = 46.9$ nm) pumped by pulse, high-current, capillary-discharge. For focusing a long-focal spherical mirror ($R = 2100$ mm) covered by 14 double-layer Sc-Si coating was used. The ablated focal spots demonstrate not only that the energy of our laser is sufficient for such experiments, but also that the design of focusing optics must be more sophisticated: severe aberrations were revealed — an irregular spot shape and strong astigmatism with astigmatic difference as large as 16 mm. In some cases, on the bottom of ablated spots a laser-induced periodic surface structure appeared. Finally, an illumination of the sample through quadratic hole 7.5×7.5 μm, standing in contact with PMMA substrate ablated from the surface a strongly developed two-dimensional diffraction pattern (period in the center about 125 nm).

Keywords: Ablation by EUV radiation; Application of Ar^{8+} laser; Nano-patterning by EUV radiation; Nano-structuring by EUV radiation

INTRODUCTION

For a long time, micro- and nano-patterning of solid surfaces was motivated by a progress in microelectronics, which, following Moore's (1975) law (doubling every two years the transistor-count that can be placed inexpensively on integrated circuit), commands[1] a continuous upgrade of lithography.[2] Such upgrade indirectly influences processing speed, memory capacity, number and size of pixels in sensors, etc. However, at present the pre-competitive cooperation phase in extreme ultraviolet (EUV) lithography is over and a few main players solve, how to expose 300-millimeter-diameter wafers with throughput about 100 wafers/h; in other words, how to ensure on these wafers an energy density 15–20 mJ/($cm^2 \cdot$ shot of EUV radiation), i.e., average EUV power 200 W at the source. This is beyond possibilities of any EUV laser.[3] However, even now, when Moore' law still holds, there is a notion that some other limit is behind the door (Hecht, 2011): in the mid-2000s, microprocessor clock rates stalled near 3 GHz because faster processors generated more waste heat than they could dissipate. Manufacturers got

Address correspondence and request for reprint to: Karel Kolacek, Institute of Plasma Physics, Academy of Sciences of the Czech Republic, v.v.i., Za Slovankou 1782/3, 182 00 Prague 8, Czech Republic. E-mail: kolacek@ipp.cas.cz

[1]Although Moore's law was initially made in the form of an observation and forecast, the more widely it became accepted, the more it served as a goal for the entire industry. This drove both marketing and engineering departments of semi-conductor manufacturers to focus enormous energy aiming at the specified increase so that it would be soon actually attained by one or more competitors. In this regard, it can be viewed as a self-fulfilling prophecy (Disco & van der Meulen, 1998).

[2]Here we have in mind a special branch of this technique (called sometimes micro- or nano-lithography) used for fabrication of integrated circuits and micromechanical systems. This lithography comprises many issues: light source (working in EUV/soft X-ray region), debris reduction, projection/illumination optics, mask production/inspection/repair, resist application/exposition/development/etching (not necessary in direct-writing case) etc.

[3]Optical lithography started with visible light sources, then shifted to ultraviolet lamps, 248 nm krypton-fluoride lasers, to the present 193 nm argon-fluoride laser. The next technological step was supposed to be the 157 nm molecular-fluorine laser, but problems with the calcium fluoride optics caused hesitation. Instead, developers turned to immersion lithography, which yields a sharper focus of the 193 nm line by directing the light through water. Refinements to immersion lithography allowed fabrication of circuits with a 45 nm half-pitch, and adding a trick called double-patterning shrank the half-pitch down to 32 nm in the last generation of fabrication lines that came on line in 2009. At present the winning new technology for 13.5 nm uses tin droplets of the exactly given size injected in a vacuum chamber; the droplets are hit on their trajectory by a CO_2 laser pulses of exactly given energy (average power 10–20 kW) that evaporate and ionize them.

around that performance wall by designing chips with multiple cores, processors that operated in parallel. Yet the new paradigm of multi-core processing cannot be extended too far without major changes in software and hardware. Software that now performs operations serially must be rewritten to execute operations in parallel on chips with more than 8 or 16 cores (Fuller & Millett, 2010), and integrated photonics hardware must provide that massive interconnectivity. Optics has inherently high bandwidth density, which advanced modulation formats and wavelength-division multiplexing can increase to levels far beyond the reach of electronics. Fiber-optic links are already used commercially on backplanes of high-performance computers. The next step is to bring them to the circuit board, where they are expected to be within a couple of years; integration of photonics on electronic chips would follow. Therefore, basic research will continue even in this well developed line and it is worth having a tool for fast nanopatterning that can assist electron beam lithography in production of research-oriented units. This trend has been confirmed at the end of 2010, when the Defence Advance Research Agency (USA) kicked off new Gratings of Regular Arrays and Trim Exposures program. Its goal is to develop methodologies enabling simplified circuit designs using high-resolution grating patterns that can be fabricated using either mask-based or mask-less interference lithography. Namely this attitude should ensure a low volume fabrication at advanced nodes at prices affordable e.g., for the United States Department of Defence (Freebody, 2011).

Simultaneously, there are other branches, where low-volume nanofabrication needs periodic nanostructures. One of them is plasmonics (see e.g., Maier, 2007; Zouhdi & Sihvola, 2009; Klimov, 2009), which belongs to most rapidly growing areas of physics, with possible applications ranging from sensing and biomedicine to imaging and nanotechnology (Baumberg *et al.*, 2005; Hill, 2009; Noginov *et al.*, 2009; Schuller *et al.*, 2010; Wu *et al.*, 2010), and which amply uses nanoparticles, nanorods, and nanostructures. The nanostructures consisting of multiple metallic elements with controlled relative placements (down to distances of the order of about 10 nm) provides a simple yet compelling way not only to tune the resonance frequencies of the system, but also to change the interaction strength with radiation (due to near-field coupling between neighboring units).[4] Among other research items that need nanostructures belong photonic crystals and nanophotonic materials (Campbell *et al.*, 2000; Fan, *et al.*, 2005), high density magnetic memories (Chou & Krauss, 1996; Heyderman *et al.*, 2004), miniaturized radio-frequency oscillators (Mancoff *et al.*, 2005), ultraviolet polarizer (Scing *et al.*, 1995; Pelletier *et al.*, 2008), dense gratings (for determination of ultimate resolution of new photo-resists (Hoffnagle *et al.*, 1999, 2003; Anderson & Naulleau, 2009; Naulleau *et al.*, 2009). Currently these nanostructures are fabricated by electron beam lithography and focused ion beam lithography, which is very precise, but simultaneously very slow (point-by-point etching) and expensive. That is why any alternative method is warmly welcomed.

This work presents our first step to nanostructure a solid surface by EUV radiation. We used for that a natural-pattern (laser induced periodic surface structure (LIPSS) on the bottom of ablated crater, or two-dimensional (2D) diffraction pattern in the windows of in-contact standing grid) created by single imperfectly-focused EUV laser beam.

At the next step a two-beam interaction (interference) pattern will be used, where the fringe spacing could be changed. A design work is in progress.

APPARATUS

Device

Experiments with nanostructuring of PMMA were performed on our older apparatus with capillary experiment (CAPEX, see Fig. 1 and for more detail see Kolacek *et al.* (2008*a*, 2008*b*) and Schmidt *et al.* (2005)).

The CAPEX device consists of (1) Marx generator, eight stages, erected capacity 12.5 nF, erected voltage 400 kV, stored energy 1 kJ; (2) Spacer, SF_6 filled, which separates oil filled Marx generator and water filled fast capacitor; (3) Fast coaxial capacitor, dimensions $Ø262 \times Ø158 \times 675$, capacitance 6 nF, characteristic impedance 3.37Ω; (4) Spark gap working in a self-breakdown regime; (5) Ceramic capillary, dimensions $Ø3.2 \times 232$, Ar filled; (6) Ar filling and pumping assembly, which maintains the optimum Ar pressure in the capillary and sufficient vacuum in the diagnostic and interaction part of the apparatus.

The CAPEX device is capable to deliver the current amplitude of about 50 kA after the current quarter-period lasting about 50 ns. For nanostructuring experiments the CAPEX apparatus was extended for (1) Vacuum tube with (a) fast mechanical shutter, which allows radiation to pass, but blocks particles and debris ejected from the capillary (due to their longer time-of-flight), (b) Quadrodiode, which enables after two or three shots to find the EUV beam axis and adjust accordingly the vacuum chamber; (2) vacuum chamber with multilayer mirror mechanically controlled from atmospheric side by double Cardan joints with Wilson vacuum seals; (3) interaction tube with mechanically controlled sample.

Multilayer Mirror

The design of multilayer mirror was split into two parts. The first one compared focusing properties of spherical mirror

[4]The full development of nanoplasmonics was delayed by the lack of devices that can generate coherent plasmonic fields. It was proposed that in the same way as a laser generates stimulated emission of coherent photons, a "spaser" could generate stimulated emission of localized and propagating surface plasmons (oscillations of free electrons in resonating metallic nanostructures) adjacent to a gain medium where absorption loss in metal is compensated by (even allows amplification due to) optical gain. Recently such "spaser" was realised (Zouhdi & Sihvola, 2009) with 44-nm-diameter nanoparticles with a gold core and dye-doped silica shell, where losses of localized surface plasmons were fully compensated by gain. Thus surface plasmon resonances were capable of squeezing optical frequency oscillations into a nanoscopic cavity creating a nanolaser with out-coupling of surface plasmon oscillations to photonic modes at a wavelength of 531 nm.

https://doi.org/10.1017/S0263034611000681 Published online by Cambridge University Press

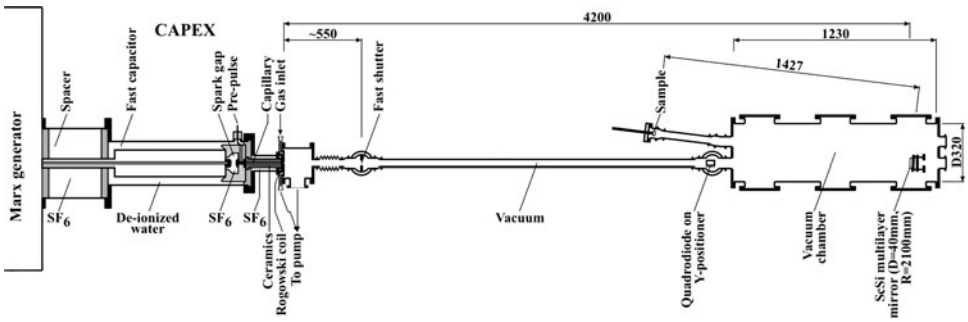

Fig. 1. Apparatus. For nanostructuring experiments the CAPEX device was extended for vacuum tube with fast shutter and quadrodiode, for vacuum chamber with multilayer mirror, and for interaction tube with sample.

with those of off-axis parabola. It turned out that for our configuration (focal length 1050 mm, angle of incident and reflected beams 7.6°) is the diameter of focal spot (where 85% of the beam-energy is concentrated) for spherical configuration about 1.5-times larger than that for the parabolic one, what was considered as acceptable for these measurements (taking also into account higher price and longer production time of the off-axis parabola).

The second part of the design concerned the Sc-Si multilayer reflecting structure. From available three references for refraction index of Si (Palik, 1985; Nielsen *et al.*, 2004; NIST, 2005) and four references for index of refraction of Sc (Vinogradov, 2002; Uspenskii *et al.*, 2004; Nielsen *et al.*, 2004; Fernandez-Perea *et al.*, 2006) those published in Nielsen *et al.* (2004), were used, namely

$$n_{\mathrm{Si}} = 0.8074 + \mathrm{i}\ 1.82\ 10^{-2},$$

$$n_{\mathrm{Sc}} = 0.96703 + \mathrm{i}\ 2.85\ 10^{-2}.$$

Reflectivity curves of multilayers were calculated with the modified software developed by Holy (FMP ChU Prague). They indicated that the best are not the layers of equal optical thickness ($n_{Sc}{}^{*}h_{Sc} = n_{Si}{}^{*}h_{Si}$, n being *Re*-part of index of refraction, h being thickness of the layer), but equal geometrical thickness ($h_{Sc} = h_{Si}$) — namely 13 nm with the tolerance +0.2 nm and −0.0 nm. The optimum number of double-layers turned to be 20 (see Fig. 2). After next two iterations that took into account production and technological possibilities our design resulted in layers of equal geometrical thickness (13.15 ± 0.3) nm, and in 14 double-layers with theoretical reflectivity 45% for perpendicular incidence.

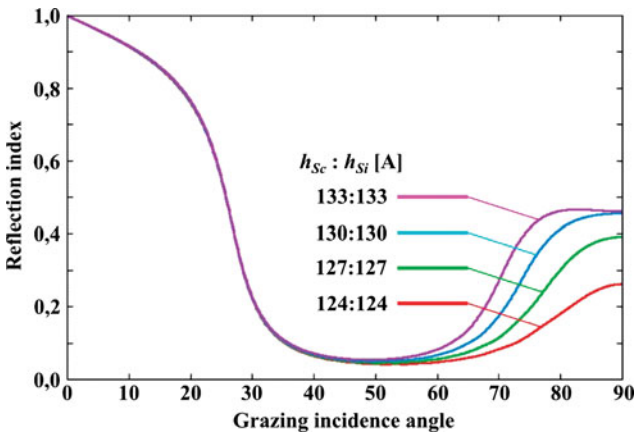

Fig. 2. (Color online) Reflectivity as a function of grazing incidence angle; parameter of curves is thickness of Sc-Si layers in Å.

ABLATION OF PMMA BY Ar^{8+} LASER BEAM

Direct Irradiation and Irradiation through a Large Grid

The sample was irradiated a few times in different positions and simultaneously photographed by photographic camera. The focused visible light emitted from the capillary was clearly visible on the PMMA surface. These spots on photographs should have assist at identification of position of ablated area. Nevertheless even at this assistance the identification of this position was extremely difficult.

The first ablated spots in PMMA (see Fig. 3) were seen in optical microscope at observation in geometrically reflected light. On the other hand, a similar observation with sample between crossed polarizers did not indicate any residual stress caused by local heating; therefore, it seems confirmed that the ablation is not a result of thermal effects of radiation, but of quantum ones only. This finding is in accord with earlier statement (Juha, *et al.*, 2005*b*; Mocek, *et al.*, 2006) that energy of EUV quanta (26.45 eV for our Ar^{8+} EUV laser) is sufficient not only for fragmentation of polymer chain, but also for releasing of atoms/fragments (mostly methyl methacrylate and CO_2) from the PMMA surface. A more detail (even still phenomenological) analysis of this process was

Fig. 3. (Color online) (**Left**) PMMA ablated by one shot of Ar^{8+} laser. (**Middle**) PMMA ablated by five shots. (**Right**) PMMA ablated through Ni grid (step 100 × 100 μm, free windows 70 × 70 μm, traverses 30 μm) by five shots; all these three pictures are in the same scale and with false colors.

https://doi.org/10.1017/S0263034611000681 Published online by Cambridge University Press

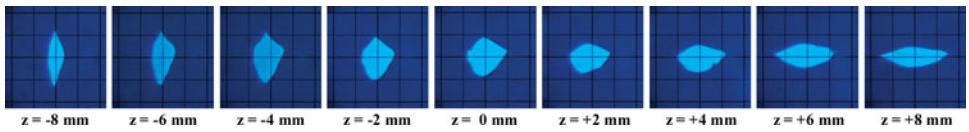

Fig. 4. (Color online) $Z-$ scan of laser beam footprint on gold-covered PMMA; apparent astigmatism is visible with astigmatic difference ~16 mm; the pictures were taken at blue illumination through microscope the measuring objective of which had grid 125×125 μm/div.

given recently by Chalupsky, *et al.* (2009). Interaction of short pulses of EUV lasers with wide band gap insulators (LiF) is described by Inogamov *et al.* (2011).

Analysis of these spots by scanning electron microscope was not successful; however, for this analysis, the PMMA sample was covered by a thin (transparent) layer of gold. Fortunately, already the first test shots at this layer showed not only that laser energy is sufficient for ablation of this layer, but also that the laser-beam-footprints are excellently visible even with the naked eye (especially if the sample is indirectly slightly back-illuminated). In this arrangement, we z-scanned the laser-beam-footprint trying to find the best focus (see Fig. 4). Despite focus of the visible light seemed to be at first glance perfect, it turned out that astigmatism of EUV radiation is very strong, astigmatic difference being about 16 mm.

Finally the laser-beam footprint was analyzed by atomic force microscope (AFM). For this analysis, two parts of the spot shown in the middle of the Figure 3 (ablation by 5 shots, about 8 mm from the central plane, i.e., in the more distant astigmatic focus) were selected: part "A" (150×150 μm) is located in the right corner of the ablated region, while part "B" (150×150 μm) is located in the middle-bottom part of that region. Part "A" as well as part "B" contains both the ablated and the not-ablated regions (see Fig. 5). It is visible that each ablated part has on its surface more or less contrast periodic structure with period about 2.8 μm and with peak-to-peak depth about 5–10 nm. It offers to attribute these structures to laser-induced periodic surface structure (LIPSS; Sipe *et al.*, 1983; Young *et al.*, 1983, 1984).

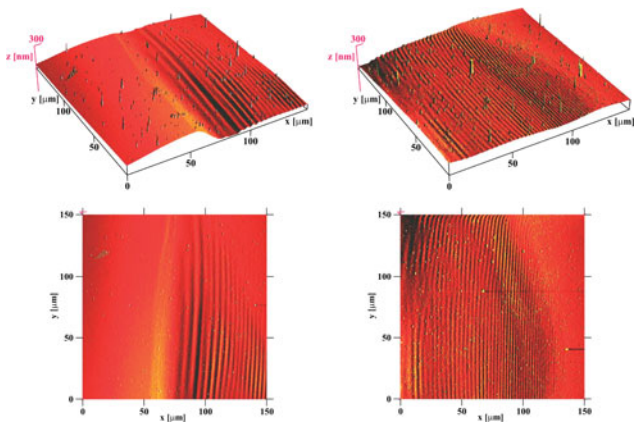

Fig. 5. (Color online) Spot ablated by five laser shots in the more distant astigmatic focus. (**Left**) region in the right corner. (**Right**) region in the middle-bottom part of the spot. (**Top**) 3D images. (**Bottom**) 2D images.

However, on the one side, LIPSS I (LIPSS of the first type) is typically created by a polarized laser light (Sipe *et al.*, 1983; representing material response to interference of the incidence radiation and the radiation scattered along the surface); contrary, amplified spontaneous emission of our mirror-less laser is not polarized and its reflection from multilayer mirror at nearly normal incidence practically does not change this fact. On the other side, the mechanism responsible for LIPSS II (LIPSS of the second type) formation is attributed to melting effects (Young *et al.*, 1984): at low fluences, the structure develops when thin molten strips resolidify on the solid substrate, while at high fluences, the structure results from freezing of capillary waves which are generated on the surface that the laser pulse has uniformly melted. Contrary, we expect that in our case the quantum ablation plays a dominant role and the thermal effects are negligible. Therefore, despite two types of LIPSS have been already classified, none of them is fully fitting to our case.

Similarly, ablation of PMMA samples with about 40 nm gold layer have also been analyzed by AFM (see Fig. 6). Left column of fields shows the upper part of the laser-beam-footprint. Both fields in this column were taken with AFM in taping mode; the upper field shows height, while the lower one shows phase contrast. Both fields indicate that in this case no periodic surface structure is created. Instead, units-of-micrometers-wide lighter part around the laser-beam-footprint in the lower field is interpreted as PMMA deposited on not-ablated gold layer. The same lighter surrounding around the laser-beam-footprint is visible in an enlarged scale in the middle-bottom-field (taken by AFM in current mode indicating local conductivity). Contrary, in the most enlarged scale (right column of the Fig. 6) no individual particles/grains/solidified-droplets of PMMA on Au were distinguishable (either in the upper field taken by AFM in taping mode measuring height, or in the lower field taken by AFM in current mode measuring local conductivity).

Irradiation through a Small Grid

Finally, a surface of bare PMMA was irradiated through a small grid (step 12.5×12.5 μm, windows 7.5×7.5 μm) closely attached to this surface (see Fig. 7) with intention to see, if some structure similar to LIPSS is generated even in a limited space like a small grid window.

Also this pattern was analyzed by AFM. It turned out that in each grid window a well-developed 2D diffraction pattern was created (see Fig. 8). The period of diffraction pattern changes from about 800 nm (at the edge of window) down

https://doi.org/10.1017/S0263034611000681 Published online by Cambridge University Press

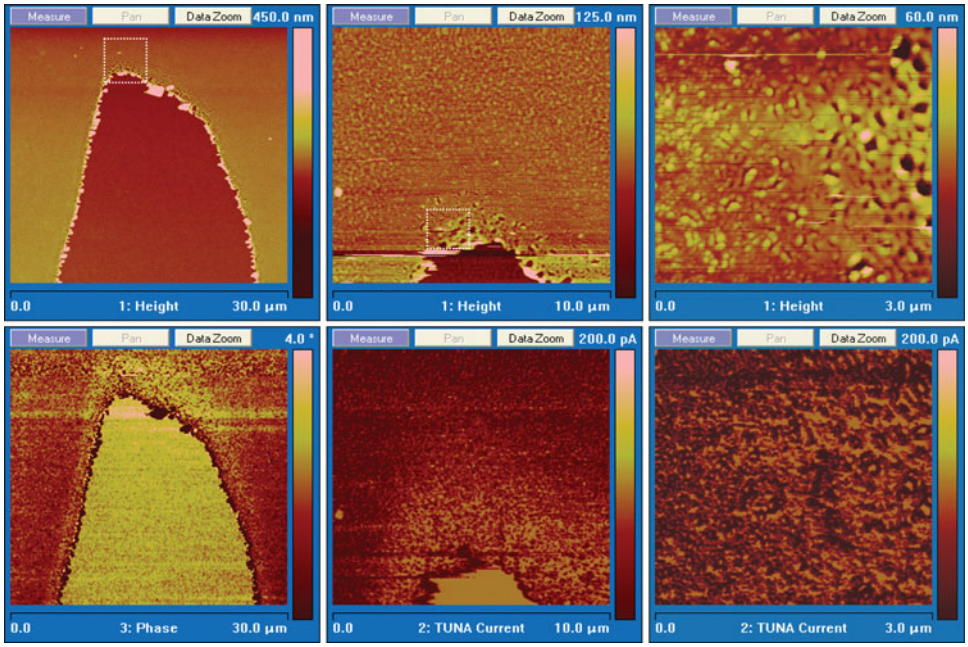

Fig. 6. (Color online) Analysis of laser-beam footprint on the gold (40 nm)-covered PMMA by AFM. (**Left Column**) upper part of the laser-beam-footprint; (**Upper Field**) AFM in taping mode indicating height; rectangle defines area shown in the middle column; (**Lower Field**) taping mode, phase contrast; (**Middle Column: Upper Field**) taping mode, height; rectangle defines area shown in the right column; (**Lower Field**) current mode. (**Right Column: Upper Field**) taping mode, height; (**Lower Field**) current mode.

to about 125 nm (in the middle of the window). One ridge (possibly a part of LIPSS) can be seen in the mid of the window.

Comparison of the ablated pattern with a theoretical profile of diffraction on a rectangular hole (see Fig. 9) confirms that the ablated pattern is really the result of diffraction.

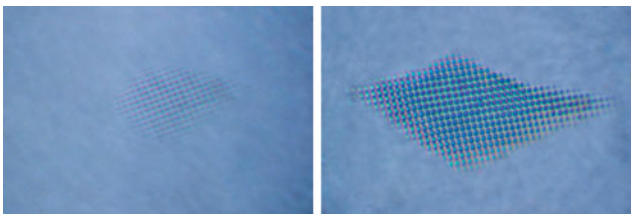

Fig. 7. (Color online) Bare PMMA ablated through the attached Au grid (step 12.5 × 12.5 µm, windows 7.5 × 7.5 µm). (**Left**) ablation by one shot. (**Right**) ablation by five superimposed shots. False colors.

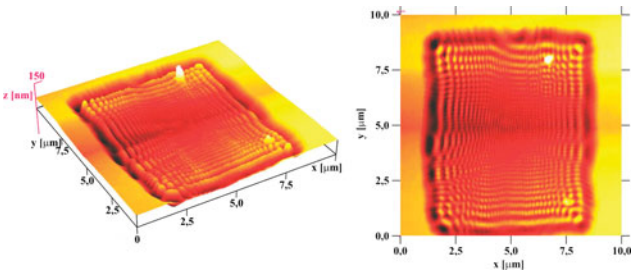

Fig. 8. (Color online) AFM analysis of the ablated pattern in one grid window (dimension 7.5 × 7.5 µm). (**Left**) 3D plot. (**Right**) 2D plot.

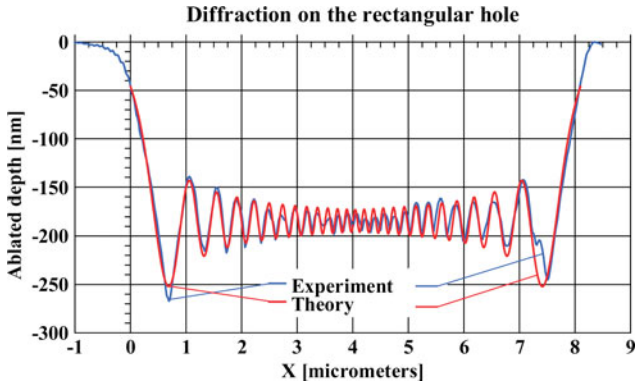

Fig. 9. (Color online) Diffraction on the rectangular hole 7.5 × 7.5 µm; horizontal profile 5.3 µm.

CONCLUSION

It was demonstrated that our EUV Ar^{8+} laser ($\lambda = 46.88$ nm), the energy of which has not yet been reliably measured, but is estimated to be tens or hundreds of µJ is capable with focused beam to ablate PMMA (similarly to Juha *et al.*, 2005*a*), even if in our case the focus is significantly influenced by astigmatisms.

If the beam-footprint on a bare PMMA surface is large, the ablated area is covered by periodic surface structure with periodicity about 2.8 µm. However, it still remains to be proved, whether this pattern can be attributed to LIPSS.

If the beam-footprint on a PMMA, covered by a thin (about 40 nm) gold-layer, is large, no periodic surface structure has been observed. Instead, around the laser-beam-footprint a

https://doi.org/10.1017/S0263034611000681 Published online by Cambridge University Press

few micrometers wide composite area is created, where gold is intermixed with PMMA.

If the beam-footprint on a bare PMMA surface is small and limited by some obstacle, a diffraction pattern is created, the periodicity of which spans down to about 125 nm.

It should be mentioned that there is only a limited possibility to change the periodicity of these surface structures (if they are created). Therefore, a new interferometer is designed, which will be able to create controlled periodic structures with periodicity approaching the laser wavelength (about 50 nm in our present case, but with perspective of further reduction Kolacek *et al.*, 2008*a*, 2008*b*, 2010).

ACKNOWLEDGMENTS

The experimental part of this work was performed under auspices and with the support of the Grant Agency of the Academy of Sciences CR (contract KAN300100702), the theoretical part of this work was supported by the Ministry of Education, Youth, and Sports of the Czech Republic (contracts LA08024 and LC528).

REFERENCES

Anderson, C.N. & Naulleau, P.P. (2009). Do not always blame the photons. Relationship between deprotection blur, line-edge roughness, and shot noise in extreme ultraviolet photoresists. *J. Vac. Sci. Technol. B* **27**, 665–670.

Baumberg, J.J., Kelf, T.A., Sugawara, Y., Cintra, S., Abdelsalam, M.E., Bartlett, P.N. & Russell, A.E. (2005). Angle-resolved surface-enhanced Raman scattering on metallic nanostructured plasmonic crystals. *Nano Lett*. **5**, 2262–2267.

Campbell, M., Sharp, D.N., Harrison, M.T., Denning, R.G. & Turberfield, A.J. (2000). Fabrication of photonic crystals for the visible spectrum by holographic lithography. *Nat*. **404**, 53–56.

Chalupsky, J., Juha, L., Hajkova, V., Cihelka, J., Vysin, L., Gautier, J., Hajdu, J., Hau-Riege, S.P., Jurek, M., Krzywinski, J., London, R.A., Papalazarou, E., Pelka, J.B., Rey, G., Sebban, S., Sobierajski, R., Stojanovic, N., Tiedtke, K., Toleikis, S., Tschentscher, T., Valentin, C., Wabnitz, H. & Zeitoun, P. (2009). Non-thermal desorption/ablation of molecular solids induced by ultra-short soft x-ray pulses. *Opt. Exp*.**17**, 208–217.

Chou, S.Y. & Krauss, P.R. (1996). 65 Gbits/in^2 quantum magnetic disk. *J. Appl. Phys*. **79**, 5066–5066.

Disco, C. & van der Meulen, B. (1998). *Getting New Technologies Together: Studies in Making Sociotechnical Order*. New York: Walter de Gruyter.

Fan, W.J., Zhang, S., Malloy, K.J. & Brueck, S.R.J. (2005). Large-area, infrared nanophotonic materials fabricated using interferometric lithography. *J. Vac. Sci. Technol. B* **23**, 2700–2704.

Fernandez-Perea, M., Larruquert, J.I., Aznarez, J.A., Mendez, J.A., Poletto, L., Malvezzi, A.M., Giglia, A. & Nannarone, S. (2006). Determination of optical constants of scandium films in the 20-1000 eV range. *J. Opt. Soc. Am. A* **23**, 2880–2887.

Freebody, M. (2011). Preserving Moore's law pushes lithography to its limits. *Photon.Spec*. **45**, 5, 45–47.

Fuller, S.H. & Millett, L.I., eds. (2010). The future of computing performance: Game over or next level? http://bit.ly/eR0e0A.

Hecht, J. (2011). Photonic integration may boost computing performance. *Laser Focus World* **47**, 57–60.

Heyderman, L.J., Solak, H.H., David, C., Atkinson, D., Cowburn, R.P. & Nolting, F. (2004). Arrays of nanoscale magnetic dots: Fabrication by X-ray interference lithography and characterization. *Appl. Phys. Lett*. **85**, 4989–4991.

Hill, M.T. (2009). Nanophotonics: Lasers go beyond diffraction limit. *Nat. Nanotechn*. **4**, 706–707.

Hoffnagle, J.J., Hinsberg, W.D., Sanchez, M. & Houle, F.A. (1999). Liquid immersion deep-ultraviolet interferometric lithography. *J. Vac. Sci.Technol. B* **17**, 3306–3309.

Hoffnagle, J.A., Hinsberg, W.D., Houle, F.A. & Sanchez, M.I. (2003). Use of interferometric lithography to characterize the spatial resolution of a photoresist film. *J. Photopoly. Sci. Techn*. **16**, 373–379.

NIST. 2005. http://physics.nist.gov/PhysRefData/FFast/html/form.html.

Inogamov, N.A., Anisimov, S.I., Petrov, Yu.V., Khokhlov, V.A., Zhakhovski, V.V., Faenov, A.Ya., Pikuz, T.A., Fortov, V.E., Skobelev, I.Yu., Kato, Y., Shepelev, V.V., Fukuda, Y., Tanaka, M., Ishino, M., Nishikino, M., Kando, M., Kawachi, T., Kishimoto, M., Nagasono, M., Tano, K., Ishikawa, T., Ohashi, N., Yabashi, M., Togashi, T. & Senda, Y. (2011). Ablation of insulators under the action of short pulses of X-ray plasma lasers and free-electron lasers. *J. Opt. Techn*. **78**, 473–480.

Juha, L., Bittner, M., Chvostova, D., Krasa, J., Otcenasek, Z., Prag, A.R., Ullschmied, J., Pientka, Z., Krzywinski, J., Pelka, J.B., Wawro, A., Grisham, M.E., Vaschenko, G., Menoni, C.S. & Rocca, J.J. (2005*a*). Ablation of organic polymers by 46.9-nm-laser radiation. *Appl. Phys. Lett*. **86**, 034109.

Juha, L., Bittner, M., Chvostova, D., Krasa, J., Kozlova, M., Pfeifer, M., Polan, J., Prager, A.R., Rus, B., Stupka, M., Feldhaus, J., Letal, V., Otcenasek, Z., Krzywinski, J., Nietubyc, R., Pelka, J.B., Andrejczuk, A., Sobierajski, R., Ryc, L., Boody, F.P., Fiedorowicz, H., Bartnik, A., Mikolajczyk, J., Rakowski, R., Kubat, P., Pina, L., Horvath, M., Grisham, M.E., Vaschenko, G.O., Menoni, C.S. & Rocca, J.J. (2005*b*). Short-wavelength ablation of molecular solids: pulse duration and wavelength effects. *J. Microlitho., Microfab.Microsys*. **4**, 033007.

Klimov, V.V. (2009). *Nanoplasmonics*. Fizmatlit: Moskva (in Russian).

Kolacek, K., Schmidt, J., Bohacek, V., Ripa, M., Frolov, O., Vrba, P., Straus, J., Rupasov, A.A. & Shikanov, A.S. (2008*a*). Amplification of spontaneous emission of neon-like argon in a fast gas-filled capillary discharge. *Plasma Phys. Rprt* **34**, 162–168.

Kolacek, K., Schmidt, J., Prukner, V., Frolov, O. & Straus, J. (2008*b*). Ways to discharge-based soft X-ray lasers with the wavelength $\lambda < 15$ nm. *Laser Part. Beams* **26**, 167–178.

Kolacek, K., Prukner, V., Schmidt, J., Frolov, O. & Straus, J. (2010). A potential environment for lasing below 15 nm initiated by exploding wire in water. *Laser Part. Beams* **28**, 61–67.

Maier, S.A. (2007). *Plasmonics: Fundamentals and Applications*. New York: Springer Science + Business Media LLC.

Mancoff, F.B., Rizzo, N.D., Engel, B.N. & Tehrani, S. (2005). Phase-locking in double-point-contact spin-transfer devices. *Nat*. **437**, 393–395.

Mocek, T., Rus, B., Stupka, M., Kozlova, M., Prag, A.R. & Polan, J. (2006). Focusing a multimilijoule soft x-ray laser at 21 nm. *Appl. Phys. Lett*. **89**, 051501.

Moore, G.E. (1975). Progress in digital integrated electronics. *Electron Devices Meeting*, 11–13.

Moore, G.E. (1965). Cramming more components onto integrated circuits. The experts look ahead. *Electron*. **38**, 8.

Naulleau, P.P., Anderson, C.N., Chiu, J., Dean, K., Denham, P., George, S., Goldberg, K.A., Hoef, B., Jones, G., Koh, C., La Fontaine, B., Ma, A., Montgomery, W., Niakoula, D., Park, J.O., Wallow, T. & Wurm, S. (2009). Latest results from the SEMATECH Berkeley extreme ultraviolet microfield exposure tool. *J. Vac. Sci. Techn. B* **27**, 66–70.

Nielsen, J., Jankowski, A., Friedman, L. & Walton, C.C. (2004). Developing multi-layer mirror technology near 45 nm using Sc/Si interfaces. Report UCRL-TR-202362. Livermore, CA: Lawrence Livermore National Laboratory.

Noginov, M.A., Zhu, G., Belgrave, A.M., Bakker, R., Shalaev, V.M., Narimanov, E.E., Stout, S., Herz, E., Suteewong, T. & Wiesnar, U. (2009). Demonstration of spacer-based nanolaser. *Nat.* **460**, 1110–1112.

Palik, E.D. (1985). *Handbook of Optical Constants of Solids*. New York: Academic Press.

Pelletier, V., Asakawa, K., Wu, M.S., Adamson, D.H., Register, R.A. & Chaikin, P.M. (2008). Aluminum nanowire polarizing grids: Fabrication and analysis. *Appl. Phys. Lett*. **88**, 211114.

Schmidt, J., Kolacek, K., Straus, J., Prukner, V., Frolov, O. & Bohacek, V. (2005). Soft X-ray emission of fast-capillary-discharge device. *Plasma Devices Operat*. **13**, 105–109.

Schuller, J.A., Barnard, E.S., Cai, W.S., Jun, Y.C., White, J.S. & Brongersma, M.L. (2010). Plasmonics for extreme light concentration and manipulation. *Nat. Mater*. **9**, 193–204.

Scime, E.E., Anderson, E.H., McComas, D.J. & Schattenburg, M.L. (1995). Extreme-ultraviolet polarization and filtering with gold transmission gratings. *Appl. Opt*. **34**, 648–654.

Sipe, J.E., Young, J.F., Preston, J.S. & Vandriel, H.M. (1983). Laser-induced periodic surface structure. 1. Theory. *Phys. Rev. B* **27**, 1141–1154.

Uspenskii, Y.A., Seely, J.F., Popov, N.L., Vinogradov, A.V., Pershin, Y.P. & Kondratenko, V.V. (2004). Efficient method for determination of extreme-ultraviolet optical constants in reactive materials: application to scandium and titanium. *J. Opt. Soc. Am. A* **21**, 298–305.

Vinogradov, A.V. (2002). Multilayer X-ray optics. *Quan.Electron*.**32**, 1113–1121.

Wu, W., Bonakdar, A. & Mohseni, H. (2010). Plasmonic enhanced quantum well infrared photodetector with high detectivity. *Appl. Phys. Lett*. **96**, 161107.

Young, J.F., Preston, J.S., Vandriel, H.M. & Sipe, J.E. (1983). Laser-induced periodic surface structure. 2. Experiments on Ge, Si, Al, and brass. *Phys. Rev. B* **27**, 1155–1172.

Young, J.F., Sipe, J.E. & Vandriel, H.M. (1984). Laser-induced periodic surface structure. 3. Fluence regimes, the role of feedback, and details of the induced topography in germanium. *Phys. Rev. B* **30**, 2001–2015.

Zouhdi, S. & Sihvola, A. (2009). Metamaterials and Plasmonics: Fundamentals, Modelling, Applications. *Proc. of the NATO Advanced Research Workshop on Metamaterials for Secure Information and Communication Technologies*, Marrakech, Morocco, 7-10 May 2008, Springer Science + Business media B.V., Dordrecht (The Netherlands).